Aerodynamics of Generalized Bent Biconics for Aero-Assisted, Orbital-Transfer Vehicles

Carol B. Davies*
Informatics General Corporation, Palo Alto, California
and
Chul Park†
NASA Ames Research Center, Moffett Field, California

A method was developed to generate the surface coordinates of body shapes suitable for aero-assisted, orbital-transfer vehicles (AOTVs) by extending bent biconic geometries. Lift, drag, and longitudinal moments were calculated for the bodies using Newtonian flow theory. These techniques were applied to symmetric and asymmetric aerobraking vehicles, and to an aeromaneuvering vehicle with high L/D. Results for aerobraking applications indicate that a 70 deg, fore half cone angle with a spherically blunted nose, rounded edges, and a slight asymmetry would be appropriate. Moreover, results show that an aeromaneuvering vehicle with $L/D>2.0$, and with sufficient stability, is feasible.

Nomenclature

A = area projected by body (reference area)
C_d = drag coefficient
C_L = lift coefficient
D = total drag
i = index for body surface point
L = total lift
M = metacenter
N = total moment
$\hat{n}$ = body normal vector
P = surface point
p = pressure
R_{max} = maximum radius of body
R_n = blunt nose radius
S_D, S_L = average moment arms
s_D, s_L = moment arms at P
X_c = proportion of first cone length to total body length
(X_{cp}, Y_{cp}) = x and y coordinates of center of pressure
X_{sm} = initial smoothing location
V = freestream velocity vector
V_∞ = freestream velocity
α = angle of attack
α_{max} = maximum angle of attack for maintaining stability
Γ = stability parameter, $= dY_{cp}/d\alpha$
γ = specific heat ratio
δ = angle between body normal and lift direction
θ_a = aft half cone angle
θ_b = angle between fore and aft cone axes (bend angle)
θ_c = critical angle for attached shock wave
θ_f = fore half cone angle
$\theta_1, \theta_2, \theta_3$ = direction angles of body normal
ρ_∞ = freestream density
ϕ = angle between body normal and low direction
ω = edge smoothing width, $= (X_c - X_{sm})/R_{max}$

Presented as Paper 83-1512 at the AIAA 18th Thermophysics Conference, June 1-3, 1983, Montreal, Canada; submitted June 30, 1983; revision submitted Nov. 2, 1983.

*Consultant, Professional Services Operations West.
†Research Scientist.

Introduction

THE effectiveness of the Space Shuttle can be enhanced if a new type of vehicle is developed with the ability to commute between various space satellites. The altitude of satellites, or space stations, varies from the current low-Earth orbits to geosynchronous orbit. Such orbital transfer requires a vehicle that is capable of making altitude and synergetic (i.e., inclinational) orbital plane changes. The efficiency of this vehicle could be improved by making use of the Earth's atmosphere for some of its maneuvering. Such a vehicle is referred to as an aero-assisted, orbital-transfer vehicle (AOTV).[1] Several designs have been proposed for a vehicle capable of making orbital altitude changes. For altitude change alone, vehicles with low L/D, referred to as aerobraking vehicles, are currently being investigated.[1,2] However, for synergetic plane changes a more appropriate vehicle would be one with a high L/D, which is referred to as an aeromaneuvering vehicle. Little work has been done on the investigation of the aerodynamic characteristics of these bodies. A bent biconic body has been proposed as a compromise to produce a moderately high drag and a moderately high L/D.[3,4] Knowledge of the aerodynamic characteristics of a vehicle is necessary to make even a preliminary assessment of its mission performance. There is an urgent need to approximately assess a large range of possible geometries for their aerodynamic characteristics.

The purpose of the present work is to 1) develop a computer program that generates body coordinates and associated body-normal vectors for a class of body geometries; 2) generate configurations of body shapes that will have low L/D for synergetic plane changes; and 3) produce quick estimates for lift and drag coefficients, moments, and stability margins for these varying shapes.

The work is focused on three types of geometries: 1) a symmetric, spherically blunted cone with a rounded frustum; 2) an asymmetric sphere cone, also with a rounded frustum; and 3) a low-drag, high L/D lifting body. It is necessary to round the frustum for the geometries of items 1 and 2 to overcome the very high heat transfer rates at the frustum's

edge.[5] One serious problem with a symmetric shape is its lack of roll stability. An asymmetric body would have positive roll stability; this geometry is also examined in this work. It will be demonstrated that this asymmetric body can be designed with a sufficient stability for a wide range of angles of attack.

In the past, low drag and high L/D lifting bodies generally have been designed for terrestrial landing and have not been configured for stowing in the Space Shuttle. The simplest high L/D shape is a flat plate; however, it is not aerodynamically stable. To produce aerodynamic stability it is necessary to have a slight curvature on the lifting surface. Truncating a smoothed, generalized, bent biconic will produce such a body shape with high L/D and a curved lifting surface.

Calculation of Body Coordinates

The basic geometry of a generalized bent biconic is described by five variables. These are the fore half cone angle, θ_f; the aft half cone angle, θ_a; the angle between the two cone axes (bend angle), θ_b; the proportion of first cone length to total body length, X_c; and the nose radius, R_n, of the spherically blunted fore cone. Lengths are normalized with respect to the total body length measured from the apex of the first cone. Figure 1 shows a profile of a bent biconic with $\theta_f = 12.84$ deg, $\theta_a = 7$ deg, $\theta_b = 7$ deg, $X_c = 0.6$, and $R_n = 0.03$. The reference longitudinal axis is chosen to coincide with the fore cone axis. This is the x axis of the y-y-z coordinate system shown in Fig. 1. A body with these dimensions has been studied experimentally[4] and theoretically.[6] An additional feature of the code used in this study is the ability to smooth the sharp juncture between the two cones. This is controlled by an additional variable, X_{sm}, that defines the location on the x axis where smoothing is to begin. The smoothed curve is defined as a fourth-order polynomial with no first- or third-order term and with a continuous second derivative to ensure that the surface is uniquely defined by this single parameter.

These six variables can produce a wide range of body shapes; some of these examples are seen in Fig. 2. The effect of smoothing the sharp juncture can be seen in Fig. 2a. Also shown is the option of truncating the end of the body perpendicular to either cone axis. Figure 2b shows the shape generated by truncating an upper portion of a biconic body. This truncation curve may be first or second order. The symmetric body seen in Fig. 2c is obtained when using a negative aft cone angle, a large nose radius, and the smoothing modification. The dotted line shows the effect of changing the smoothing parameter. In Fig. 2d a small bend angle has been introduced to produce an asymmetric body.

The solution of the equation of the common ellipse at the intersection plane is the first step in the procedure to obtain the surface coordinates. The apex of the aft cone and other necessary parameters are then calculated and used for solving the analytical equations that describe the body surface. Cross sections are circular along the fore cone, part circular and part elliptical through the juncture area, and elliptical until the end of the body. After obtaining the body coordinates, the body-normal vector is calculated numerically at each body coordinate.

Aerodynamic Characteristics

One of the objectives of this work is to provide a quick and simple method for computing aerodynamic characteristics for a range of body shapes. This information then can be used to determine the flight performance of the vehicles. The aerodynamic characteristics are presented in terms of lift and drag forces and are chosen to facilitate flight trajectory calculations and circumvent the ambiguity of the body reference axis. The transformation from lift and drag forces to normal and axial forces is well known.

As with any atmospheric flight vehicle, an aeromaneuvering AOTV will perform in the same manner as a conventional airplane performs and, therefore, the aerodynamic definitions of lift, drag, and moment apply. For an aerobraking vehicle, the performance criteria depend strongly on the mode of control. To correct for errors in entry angle, and for the uncertainty at atmospheric density, an aerobraking vehicle must be able to vary either lift or drag during its flight. The concept of drag modulation has been proposed and investigated.[7] To modulate drag it is necessary to vary body geometry during flight, the feasibility of which has not yet been demonstrated. In the present work, the alternate concept of lift modulation is pursued. Since control surfaces are ineffective for a very blunt body, an alternative method for modulating lift must be found. The present work investigates the feasibility of maintaining the required angle of attack by means of adjusting the center of gravity location. This adjustment could be performed by a hinge or gimbal motion. The vehicle must be stable at the achieved angle of attack; that is, a moment must be produced that will restore the angle of attack to the required value. Therefore, it is necessary to know the stability characteristics of the aerobraking vehicle over a wide range of angles of attack. In this work only longitudinal stability will be fully investigated; the inclusion of roll and directional stability is not addressed at this time.

Method of Calculation

Newtonian flow theory is used in this work to approximate the pressure at each point on the body surface. This theory

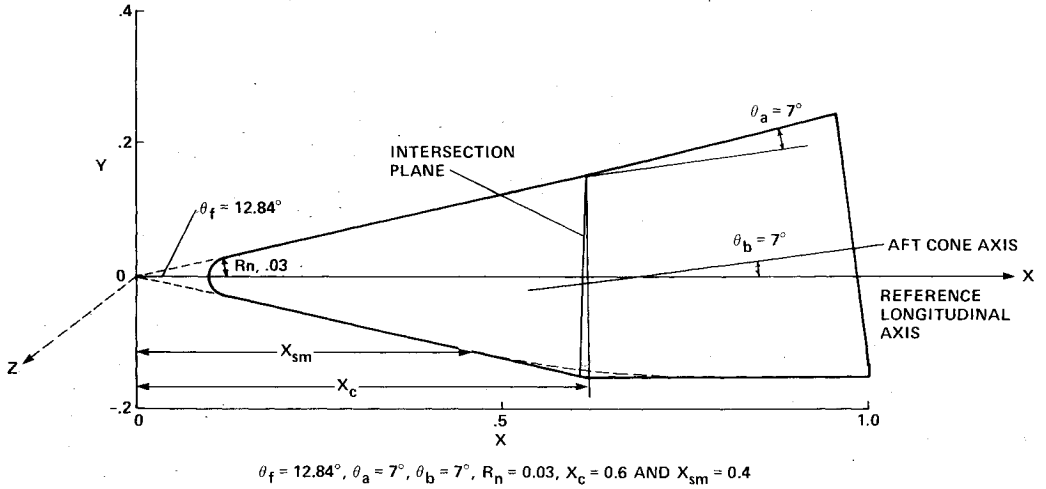

$\theta_f = 12.84°$, $\theta_a = 7°$, $\theta_b = 7°$, $R_n = 0.03$, $X_c = 0.6$ AND $X_{sm} = 0.4$

Fig. 1 Parameters of bent biconic geometry.

assumes an infinite Mach number and a specific heat ratio $\gamma = 1$. If the shock wave remains attached to the cone surface, this theory will present a reasonable approximation for pressure in the high Mach number flows encountered by an AOTV.[8] For undissociated air and $\gamma = 1.4$, the maximum cone angle for an attached shock, defined as the critical angle θ_c, is given as 57.6 deg.[9] As Mach number increases, air dissociates and γ decreases. In Ref. 8, it is shown that, for a cone flying through the atmosphere at a speed of 4.5 km/s, this critical angle is 65 deg. The relationship between shock angle θ_c and γ at infinite Mach number is given in Ref. 10. These equations were solved for varying γ and the results are shown in Fig. 3. An AOTV will be flying at 9-11 km/s, producing γ of approximately 1.1. At this value, $\theta_c = 72.5$ deg, indicating that reasonable results can be provided for fore cone angles up to this limit.

In general, a surface is defined by its normal at every point. The angle between this normal and the direction of the oncoming flow then can be found. Defining this angle at a general surface point i as ϕ_i the local pressure p_i is given by

$$p_i = \rho_\infty V_\infty^2 \cos^2(\phi_i)$$

where ρ_∞ is the freestream density and V_∞ is the freestream velocity. This expression is equivalent to the more familiar sine-squared formula.[11] Drag, which acts in the direction of the flow, is given by $p_i \cos(\phi_i)$, and lift, which acts in the direction normal to the flow, is given by $p_i \cos(\delta_i)$, where δ is the angle between the body-normal vector and the lift direction. These angles are shown more clearly in Fig. 4. It should be noted that the directions of pressure, drag, and lift do not lie in the same plane. The body-normal vector in this same coordinate system is defined as

$$\hat{n} = \cos\theta_1 i + \cos\theta_2 j + \cos\theta_3 k$$

where θ_1, θ_2, and θ_3 are direction angles with respect to the x, y, and z axes. The integrated pressure, total drag, and total lift are obtained by summing their local values over the surface area that is impinged by the flow. Newtonian flow theory dictates that only the surface area directly wetted by the flow should be included in the surface integration. A point will be on this windward side if the angle between the flow and the body normal is less than 90 deg. The drag and lift coefficients are obtained by

$$C_d = 2D/\rho_\infty V_\infty^2 A$$

and

$$C_L = 2L/\rho_\infty V_\infty^2 A$$

where D and L are the total drag and lift, and A is the area projected by the body on the y-z plane.

Two cases were run to check the accuracy of the results obtained using this method. The first was simply to check the code by calculating the drag coefficients of single cones with large nose radii. An excellent match was obtained when these were compared with the analytically derived drag coefficients for the same body dimension. In the second test case, comparisons were made with the experimental results at Mach 6 for the bent biconic body shown in Fig. 1. Figure 5 shows drag and lift coefficients vs angle of attack for both methods. It can be seen that both agree to within approximately 5%. The L/D values agree extremely well. The small discrepancies can be attributed mainly to the non-Newtonian flow in the experiment.

The diagram in Fig. 6 illustrates the technique used to compute the lift and drag moments of the body. Each surface point (shown as P in the diagram) is projected on the x-y plane. The moments for this projected line are taken about the system origin, where s_L is the moment arm for lift and s_D is

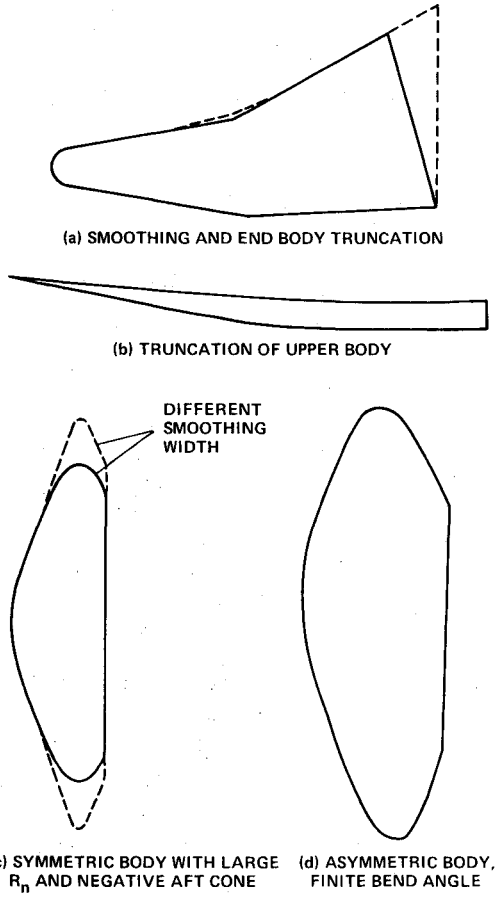

Fig. 2 Generalized bent biconic body shapes.

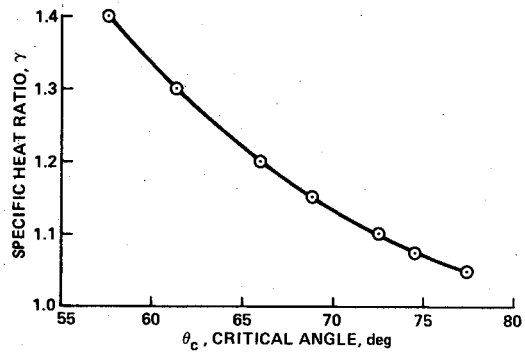

Fig. 3 Upper limit of fore cone angle for attached shock.

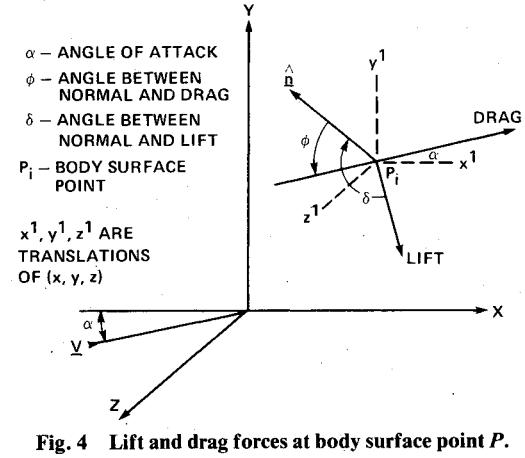

Fig. 4 Lift and drag forces at body surface point P.

the moment arm for drag. The total moments are found by summing each local moment over the appropriate body surface area, that is, total lift moment, $N_L = \Sigma s_{L_i} L_i$, and total drag moment, $N_D = \Sigma s_{D_i} D_i$. The signs of each s_L and s_{D_i} must be monitored carefully. The center of pressure (X_{cp}, Y_{cp}) is found by computing the average arm length by $S_L = N_L/L$ and $S_D = N_D/D$. These are then translated into the x-y plane. The computed horizontal center of pressure (X_{cp}) for each angle of attack is compared with the experimental results of Ref. 4 and plotted in Fig. 7. There is a discrepancy, however, that can be attributed partly to the unsuitability of the Newtonian flow for a body with a sharp junction point. At such a juncture point, pressure transmission within the boundary layer reduces the pressure difference between the two surfaces. Although this phenomenon has a minimal effect on the total lift or drag, it does influence the moments. However, for the smooth surfaces considered in the remainder of this work, such discrepancies will be negligible.

The next step is to obtain permissible locations for the center of gravity. To do so, the center of pressure is plotted for each angle of attack. The resultant force line of the lift and drag forces that acts at the center of pressure is now drawn. Figure 8 shows examples of these lines. The point at which the resultant force meets the longitudinal axis is called the metacenter, M. To produce a particular angle of attack, the center of gravity should lie along the force line. The vehicle must be able to restore itself if a correction to angle of attack is required. A change in angle of attack will produce a change in the center of pressure and, consequently, a change in the force line. This new force line will produce a moment in the restoring direction as long as the rate of change of Y_{cp} with respect to α (called the stability parameter, and defined as Γ) remains sufficiently large and negative. The maximum angle of attack up to which Γ maintains this condition will be referred to as α_{max}. The force line at α_{max} therefore will be the upper limit for the location of the center of gravity. The longitudinal location for the center of gravity is bounded by X_{cp} and M of this same force line. The quantities Γ, α_{max}, and M therefore completely determine the stability characteristics of a vehicle and will be referred to frequently in the next section.

The code was written in FORTRAN for a DEC VAX/VMS system, and the average run time for a complete case was under 2 min.

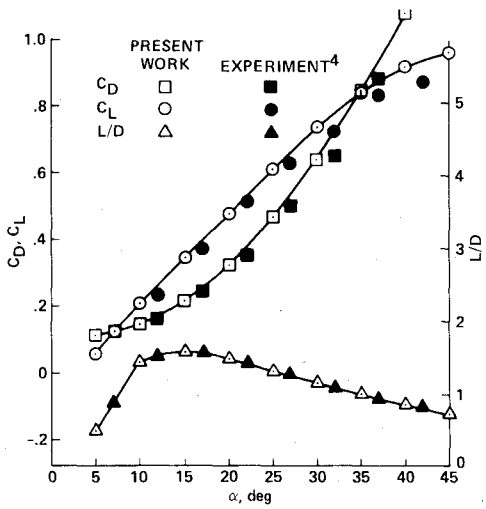

Fig. 5 Comparison of lift and drag coefficients and L/D with experimental results for body shown in Fig. 1.

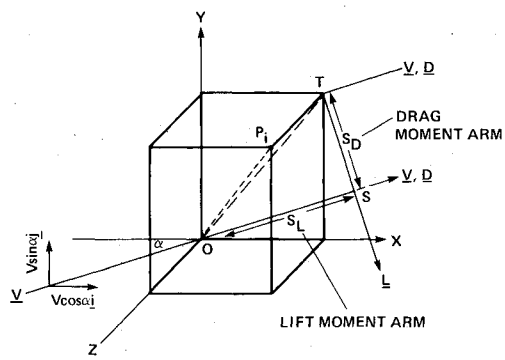

Fig. 6 Computation of moments; OT is the projection of OP onto the x-y plane.

Results

Aerobraking Vehicles

The aerodynamic characteristics computed for one case of a typical symmetric body are described first. Several parameters are then varied to provide information for generating an optimum body shape. The results of these variations (see Figs. 9-11) have been normalized with respect to the maximum radius R_{max} of the body so that the results are presented in a comparable form for each body shape.

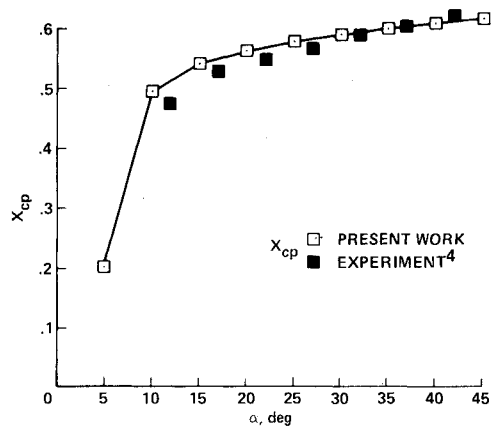

Fig. 7 Comparison of calculated center of pressure with experimental data for body in Fig. 1.

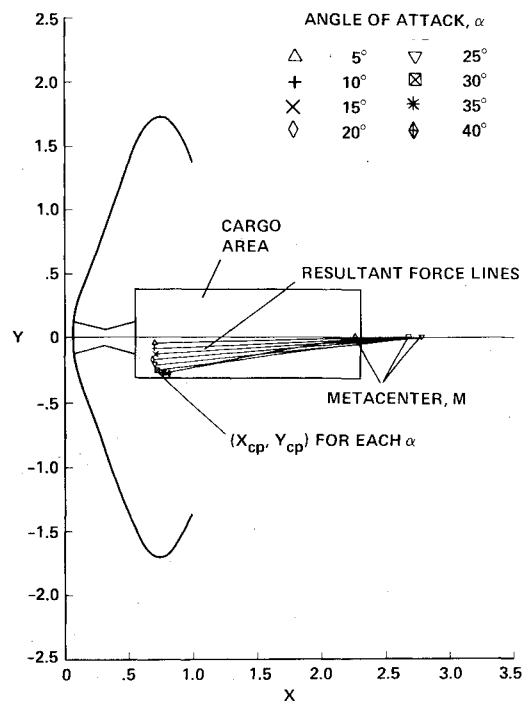

Fig. 8 Symmetric aerobraking body with $\theta_f = 70$ deg, $R_n/R_{max} = 0.6$, and $X_{max}R_{max} = 0.24$.

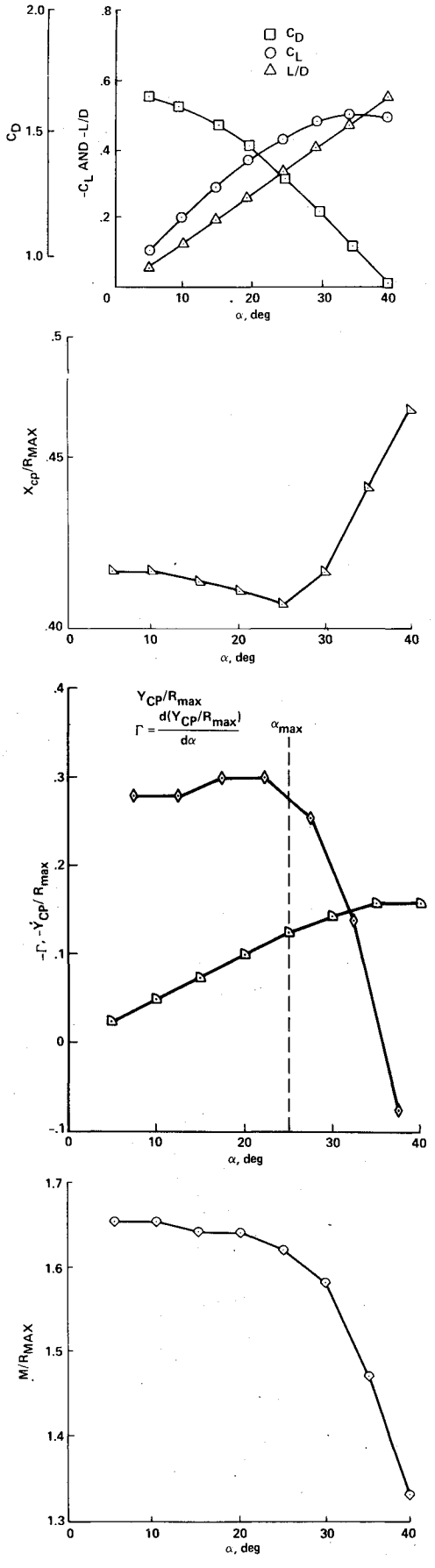

Fig. 9 Aerodynamic characteristics of body in Fig. 8.

Symmetric Body Shape

A symmetric body with a rounded frustum is seen in Fig. 8, with $\theta_f = 70$ deg, $\theta_a = -70$ deg, $R_n = 0.6$, and $X_{sm} = 0.24$. The lift and drag coefficients and L/D were computed for angles of attack between 0 and 40 deg and are shown in Fig. 9a. A fore cone angle >45 deg will produce negative lift values; the absolute values will be used in this report. C_d varied from 1.6 at $\alpha = 5$ deg to 0.9 at $\alpha = 40$ deg, and $|C_L|$ varied between 0.1 and 0.5 for the same range. $|L/D|$ varied from a minimum of 0.07 at $\alpha = 5$ deg, to a maximum of 0.57 at α deg. The variation of the center of pressure (X_{cp}, Y_{cp}) is seen in Figs. 9b and 9c. X_{cp} remained fairly constant at approximately 0.41 up to $\alpha = 30$ deg, and then increased rapidly to 0.46 at $\alpha = 40$ deg. Y_{cp} decreased linearly up to $\alpha = 30$ deg and then flattened out. In Fig. 9d, M remained between 1.6 and 1.65 up to $\alpha = 25$ deg and then decreased rapidly. The stability parameter shown in Fig. 9c also remained fairly constant up to 25 deg with a value of approximately 0.29; however, the decrease that is seen for 25 deg $< \alpha < 30$ deg indicates that this is the maximum α for maintaining stability. From these results, the maximum angle of attack (α_{max}) for this body shape is close to 25 deg. At α_{max}, $|L/D| = 0.35$.

To assess the effect of change on the nose radius, cases were run for R_n/R_{max} varying from 0.3 to 2.4, with all other parameters unchanged. The results were quite similar to the case already described. Figure 10a illustrates that although the stability parameter was a maximum for $R_n/R_{max} = 1.0$, the overall change was not significant until $R_n/R_{max} > 2.0$. Plotted on the same graph is the variation M with respect to R_n/R_{max}. Initially, M also remained fairly constant, then increased for the larger nose radii. Both curves are only valid up to α_{max}. $|L/D|$ at α_{max} varied very little, maintaining a value between 0.35 and 0.37. These results indicate that the nose radius has little effect on the large characteristics of the body, although Γ does decrease for large values of R_n/R_{max}.

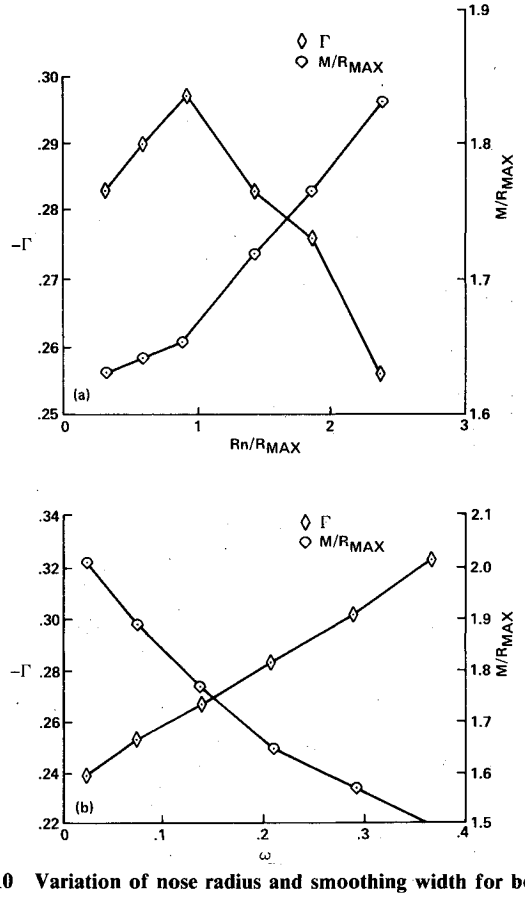

Fig. 10 Variation of nose radius and smoothing width for body in Fig. 8.

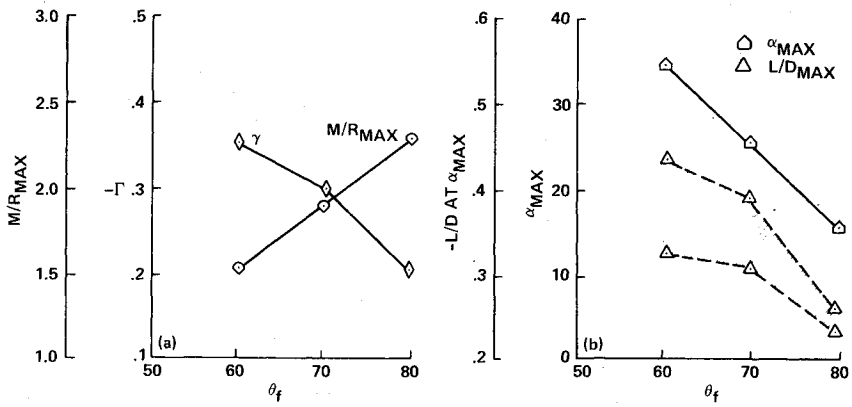

Fig. 11 Effect of change in half cone angle for symmetric bodies.

Another body parameter of interest is the roundness of the frustum edge. The change is radius of curvature is controlled by X_{sm}/R_{max}, the location where smoothing is to begin. The smoothing width, $\omega=(X_c-X_{sm})/R_{max}$, is the distance between the cut line and X_{sm}, and as this decreases, the frustum edge becomes sharper, that is, the smallest X_{sm} produces the most rounded edge. This effect can be seen in Fig. 2c where the solid line was produced by a greater smoothing width than the dotted line. Cases were run varying ω from 0.08 to 0.38. The results of this variation can be seen in Fig. 10b. As ω increased Γ also increased, indicating that the more rounded frustum edge produced a significantly more stable body. At the same time, M decreased. This implies that the more stable bodies have a smaller range for locating the center of gravity. The maximum angle of attack remained at 25 deg, whereas $|L/D|$ varied from 0.31 for the most rounded edge to 0.39 for the sharpest.

Increasing or decreasing the fore half cone angle θ_f had a significant effect on the range of the stability parameter and the location of M. Cases were run for $\theta_f=60$ and 80 deg for comparison with the 70 deg results above. It was difficult to match the body dimensions for true comparisons; nevertheless, a clear picture emerged. Figure 11 shows some interesting results. With increasing θ_f, M increased from 1.5 at 60 deg to 2.25 at 80 deg (Fig. 11a), whereas Γ decreased from 0.35 to 0.19 (Fig. 11b). Even more interesting, α_{max} increased to 35 deg for $\theta_f=60$ deg and decreased to a very low 15 deg for the 80 deg case. As a consequence, $|L/D|$ at α_{max} is greatest for the 60 deg case (Fig. 11b). The range of $|L/D|$ was more dependent on the body shape than on the other variables; Fig. 11b also indicates the range of $|L/D|$ for each cone angle.

These data show that the fore cone angle has a significant effect on the stability of the vehicle. An angle of 70 deg appears to be the optimum fore cone angle for this type of aerobraking vehicle. A fore cone angle of 60 deg restricts the location of the center of gravity to a fairly small range, however, it has a greater stability parameter. For the 80 deg case, $\alpha_{max}=15$ deg would almost certainly be too low.

Asymmetric Body Shape

The characteristics of axially asymmetric bodies also were examined in this work. Figure 12 is a profile of such an asymmetric body with $\theta_f=70$ deg, $\theta_a=-70$ deg, $\theta_b=5$ deg, $R_n=0.96$, and $X_{sm}=0.26$. Because of asymmetry, the characteristics were evaluated for angles of attack between -40 and $+40$ deg. The values computed for C_d, $|C_L|$, and $|L/D|$ were very close to the values for the similarly proportioned symmetric case. The M for each force line no longer lies on the longitudinal axis as this is not the symmetric axis of the body. In this figure, M lies above the longitudinal axis at a point where most of the force lines meet. This is at a value approximately equal to 1.6. Figure 13 is a plot of Γ vs angle of attack. Between -25 deg $<\alpha<25$ deg the stability

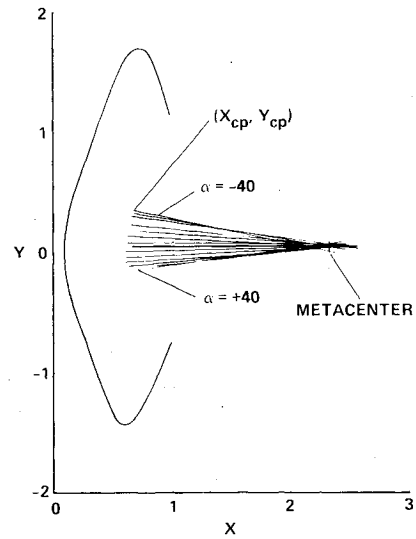

Fig. 12 Asymmetric body with $\theta_f=70$ deg, $\theta_b=5$ deg, $R_n=0.96$, $X_{sm}=0.26$.

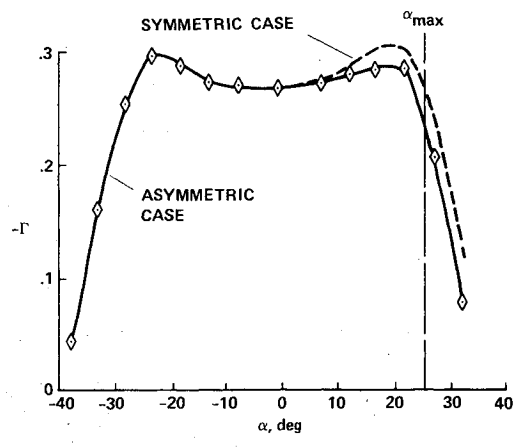

Fig. 13 Stability parameters for body in Fig. 12.

parameter remained fairly constant at a value $\cong 0.28$, again indicating an $\alpha_{max}\cong 25$ deg.

To find the effect of changing the bend angle, the same case was run for $\theta_b=3$, 7, and 10 deg. When the stability parameters were compared with the 5 deg case, very little change had occurred; Γ remained between 0.27 and 0.28. The M slightly increased with increasing bend angle. This indicates that the bend angle probably can be chosen to best suit the other requirements of the vehicle, particularly for maintaining its roll stability. The amount of bend angle required for this roll stability needs further investigation.

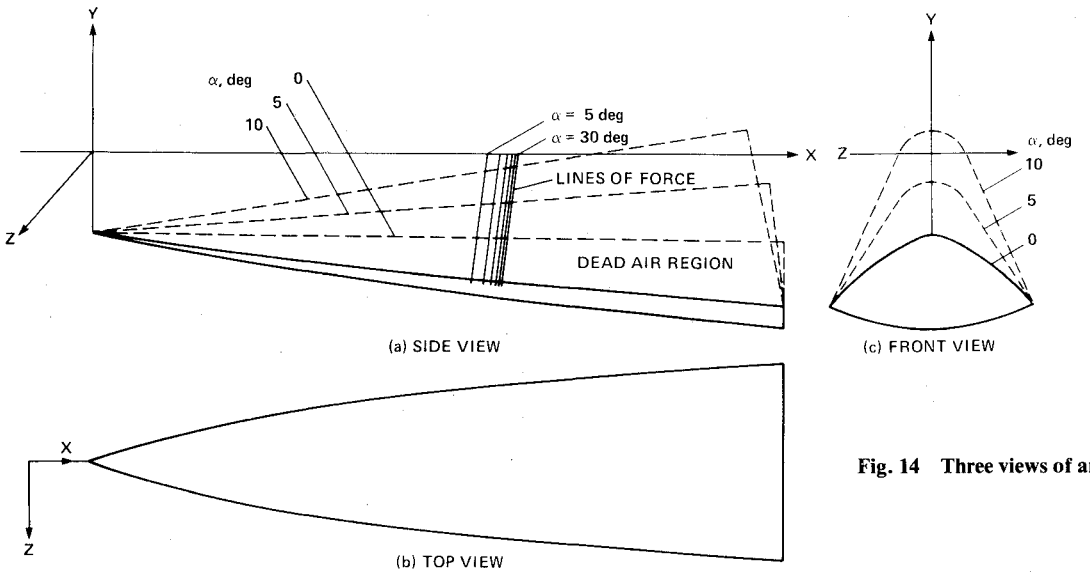

Fig. 14 Three views of an aeromaneuvering vehicle.

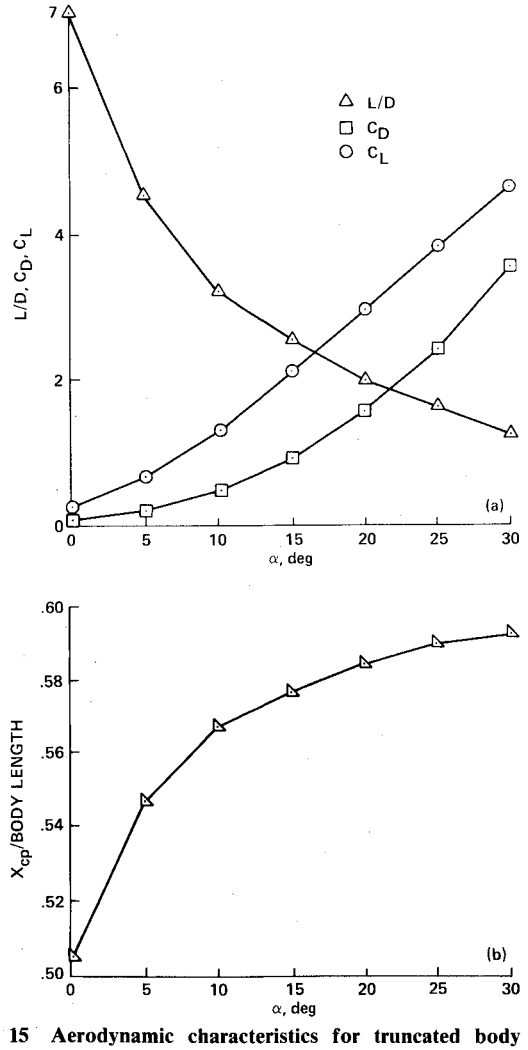

Fig. 15 Aerodynamic characteristics for truncated body shown in Fig. 14.

The effect of a fore cone angle change was investigated also, and, as in the symmetric case, exact comparisons could not be made. However, the same general picture was produced: The larger cone angle of 60 deg generated a larger stability derivative and a smaller M. The range for α_{max} again ran from 35 deg for $\theta_f = 60$ deg to 15 deg for $\theta_f = 80$ deg.

In conclusion, the introduction of a small bend angle to a symmetric aerobraking vehicle will have little effect on the longitudinal stability.

Aeromaneuvering Vehicle

The concept of creating a high lift, high L/D vehicle by truncating a bent biconic body was introduced earlier in this report. This truncated body is the lower segment of the intersection of a second-order equation with a bent biconic body. The equation is defined by three given points on this upper surface. The finalized body shape must fulfill several requirements: 1) The body should be proportioned for utilizing the cargo bay of the Space Shuttle (approximately 20×5 m) as efficiently as possible. 2) The rear side area must be large enough to produce yaw and roll stability. 3) The under surface must be sufficiently curved to produce longitudinal stability.

One possible body shape, created with these constraints in mind, can be seen in Fig. 14. The biconic surface was generated from a body with $\theta_f = 10$ deg, $\theta_a = 10$ deg, $\theta_b = 5$ deg, $X_{sm} = 0.4$, and $X_c = 0.6$. The three points defining the upper surface equation were $(0.3, -0.05)$, $(0.06, -0.095)$, and $(1.0, -0.13)$. The three views of the body seen in Fig. 14 are plotted to the same scale. The lower curved surface can be seen with the greatest volume in the rear (Fig. 14a). It is clear that the sharp leading edges will require some form of active cooling. The upper dotted portion, which indicates the dead-air region at $\alpha = 0$, can be filled without affecting the aerodynamic characteristics. This dead-air region would increase when the vehicle flies at a finite angle of attack. Also shown are the force lines for 5 deg $< \alpha <$ 30 deg. Figure 14b is the view from above, showing a large area on the upper surface, and Fig. 14c is the view from the front, showing the area projected on the y-z plane. Figure 15 details the aerodynamic characteristics computed for this aeromaneuvering vehicle. In Fig. 15a, the range of L/D is from 7.2 at zero angle of attack to 1.4 at $\alpha = 30$ deg. A sufficient spread in X_{cp} is required to provide the required stability margin. The computed values of X_{cp} presented in Fig. 15b indicates a sufficient spreading up to an α_{max} approximately equal to 20 deg. At this α_{max}, L/D still maintains a value of 2.0.

The volume to carry fuel and cargo must be found within the dead-air region on the lee side of the vehicle. The actual cargo-carrying volume will be determined by the intended maximum L/D: the higher this L/D, the smaller the angle of attack, leading to a smaller cargo volume. Eventually, the cargo-carrying volume will be so small that the vehicle will be unable to carry all of its own fuel internally. Additional fuel

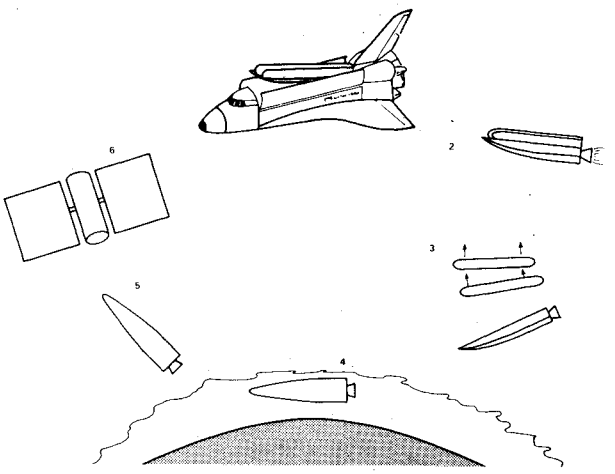

Fig. 16 Aeromaneuvering mission.

could be provided by external fuel tanks. Finally, a sequence of events is proposed for the vehicle to perform its journey from the Space Shuttle to another orbiting body. These steps, shown in Fig. 16, are:

1) The vehicle is deployed from the Shuttle cargo bay, with the external fuel tanks attached.

2) The rocket engines ignite and the vehicle begins its journey toward the Earth's atmosphere.

3) The empty fuel tanks are jettisoned and the vehicle enters the atmosphere.

4) Using its designed maneuvering capabilities, the vehicle banks and turns into its new orbit.

5) The vehicle exits the atmosphere and rendezvouses with a satellite.

Because of the large L/D of this vehicle, the required amount of fuel for performing aeromaneuvering will be quite small. It even may be possible to make two plane changes in one mission, thereby enabling the vehicle to reach its destination and return to the Space Shuttle.

Conclusions

Symmetric and asymmetric aerobraking bodies and an aeromaneuvering body can be generated by generalized bent biconic geometry. The aerodynamic characteristics derived for these bodies using Newtonian flow theory were shown to be sufficiently accurate for preliminary design studies.

For aerobraking bodies, a 70 deg half cone angle provided the best compromise between longitudinal stability and center of gravity location. The introduction of a small asymmetry to a symmetric body had little effect on the aerodynamic characteristics. For an aeromaneuvering vehicle, it is possible to design a body that has an $L/D>2$ and which can still maintain a positive stability margin.

References

[1]Walberg, G. D., "A Review of Aeroassisted Orbit Transfer," AIAA Paper 82-1378, Aug. 1982.

[2]Schmitt, D. A., "Base Heating on an Aerobraking Orbital Transfer Vehicle," AIAA Paper 83-0408, Jan. 1983.

[3]Florence, D. E., "Aerothermodynamic Design Feasibility of a Generic Planetary Aerocapture/Aeromaneuver Vehicle," AIAA Paper 81-1127, June 1981.

[4]Miller, C. G., Blackstock, T. A., Helms, V. T., and Midden, R. E., "An Experimental Investigation of Control Surface Effectiveness and Real-Gas Simulation for Biconics," AIAA Paper 83-0213, Jan. 1983.

[5]Kemp, N. H., Rose, P. H., and Detra, R. W., "Laminar Heat Transfer Around Blunt Bodies in Disassociated Air," *Journal of Aeronautics and Space Sciences,* Vol. 26, No. 7, July 1959.

[6]Swaminathin, S., Kim, M. D., and Lewis, C. H., "Three-Dimensional Nonequilibrium Viscous Shock-Layer Flows over Complex Geometries," AIAA Paper 83-0212, Jan. 1983.

[7]Andrews, D. G., Caluori, V. A., and Bloetscher, F., "Optimization of Aerobraked Orbital Transfer Vehicles," AIAA Paper 81-1126, June 1981.

[8]Feldman, S., "Hypersonic Conical Shocks for Dissociated Air in Thermodynamic Equilibrium," *Jet Propulsion*, Vol. 27, Dec. 1957, pp. 1253-1255.

[9]Macoll, J. W., "The Conical Shock Wave Formed by a Cone Moving at High Speed," *Proceedings of the Royal Society, London,* Series A, Vol. 159, 1937, pp. 459-472.

[10]Berger, S. A., "Hypersonic Flow Over Cones," AFOSR TN 60-1214, Rept. 523, Sept. 1960.

[11]Hayes, D. W. and Probstein, R. F., "Hypersonic Flow Theory," *Applied Mathematics and Mechanics,* Vol. 5, 1959, p. 73.